Investigations of the ballistic response of hybrid composite laminated structures

L. Peng[a,b], M.T. Tan[c], X. Zhang[c*], G. Han[c], W. Xiong[c], M. Al Teneiji[d], Z.W. Guan[b,d,e*]

[a] *University of Science and Technology Park, Guiyang University, Guiyang 550005, PR China*

[b] *School of Engineering, University of Liverpool, Liverpool L69 3GH, United Kingdom*

[c] *School of Mechanical Engineering, Nanjing University Science & Technology, Xiaolingwei 200, Nanjing 210094, China*

[d] *Advanced Materials Research Centre, Technology Innovation Institute, Abu Dhabi, United Arab Emirates*

[e] *School of Mechanical Engineering, Chengdu University, Chengdu, 610100, China*

* E-mail address: lynx@njust.edu.cn (Xianfeng Zhang); zhongwei.guan@liverpool.ac.uk (Zhongwei Guan).

**Abstract**

Classic lightweight composite armour systems are usually made of ceramics, metals and fabric laminates separately or combination of two materials to resist a ballistic impact by 7.62 mm projectile. To enhance the ballistic impact resistance, this paper proposes hybrid laminated structures, which are developed through combinations of ceramics, Dyneema, Kevlar and compressed wood. There were twenty-five hybrid ballistic panels manufactured first, which were then subjected to field ballistic tests with 7.62 mm (×39 mm) bullets in a velocity range from 806.0 to 887.5 m/s. Here, five of twenty-five panels successfully stopped 7.62 mm projectile. The results of the ballistic performance, energy absorption, back face signature and failure mode of each type of the composite panels were obtained and examined. The mechanisms of ballistic resistance associated with different hybrid panels designed are investigated and discussed. In addition, analytical models are developed to predict ballistic perforation performance of single material layers and the related hybrid composite structures. The theoretical predictions of residual velocities are compared with the corresponding experimental measurements in a good agreement. These results provide the first-hand data to support further concept design of the hybrid ballistic panels and to validate computer models for optimizing lightweight composite armour.

Keywords: Ballistic impact; Hybrid laminates; Ceramic; Fabrics; Compressed wood

# 1 Introduction

Composite materials are increasingly used in aerospace, automotive, infrastructure and military industries. Laminated composite material is one of the composite materials, which consists of several laminates of same fibre reinforced plies or hybrid laminates with at least two different materials, bonded with each other to form a multilayer structure. Hybrid laminated structure can be used to significantly improve the strength, fatigue life, corrosion resistance, stiffness, thermal and acoustic insulation, with a low self-weight [1]. Different from common laminates, an effective ballistic composite laminate is usually made of two primary layers to resist ballistic impact, one is a relatively hard facing plate, and the other is a relatively tough backing plate [2-9]. In general, during ballistic impact it is desired that the bullet can be blunt and eroded when striking a hard plate, and the tough backing material can support the ceramics and efficiently absorb the energy during the bullet penetration [10-13]. Wood is one of natural materials, which is widely used in building structures [14-16]. In general, the wood has high stiffness- and high strength-to-weight ratios as one of environmentally friendly and economically beneficial construction materials [17-21]. To improve mechanical properties of wood, densification technology can be used to enhance the mechanical properties of virgin wood by decreasing the pores and voids between cell walls [20-21]. Basically, the only effective direction for densification is the radial direction of wood, through which a flatten compressed wood piece can be obtained without any fracture [22]. Sanborn et al. [23] undertook ballistic tests using a powder gun on two different softwood (Spruce Pine Fir South (SPF-S) and the Southern Yellow Pine (SYP) by using a 12.7 mm steel sphere projectile made of hardened impact-resistant S-2 tool steel. The dimensions of the CLT (cross laminated timber) panel were 305 mm×305 mm, the thickness varied in the number of plies, and the majority of striking velocities was less than 762 m/s. When the striking velocity was around 800 m/s and thickness was 5-ply (thickness=175 mm), the average residential velocity of SPF-S and SYP were 400 m/s and 300 m/s, respectively. The experimental results showed that the ballistic performance of the SYP was better than the SPF-S specimens with varying thickness. However, according to the authors' best knowledge, it seems no work being carried out on ballistic tests of compressed wood.

Liu et al. [11] carried out a series of high velocity ballistic experiments on alumina ceramic composite armour with a tough backing material. They found the 18 mm thick alumina ceramic layer with a 10 mm back laminate of Ti6Al4V/UHMWPE/Ti6Al4V could resist a 12.7 mm armour piercing projectile with an impact velocity of about 800 m/s. The middle UHMWPE (Ultra High Molecular Weight Polyethylene Fibre) layer showed a high buffer performance and had a good energy balance function between the first and outermost Ti6Al4V layers. Shen et al. [12] undertook the high velocity ballistic experiments on SiC ceramics/UHMWPE composite laminates. Based on the sensitivity analysis of material and adhesive parameters by using a validated numerical model, the bulging deformation decreased with increasing the adhesive strength. Therefore, the adhesive strength could be taken as a reliable constraint to achieve the minimum bulging deformation and the minimum laminate thickness. Based on the experimental investigations by Maffeo and Cunniff [24], the ceramic layer and Kevlar29 composite laminates with polyethylene resin had a higher ballistic performance than using PVB-phenolic resin. However, the ceramic layer and Kevlar KM2 composite laminates with PVB-phenolic resin had a higher ballistic performance than the laminates with polyethylene resin. Krishnan et al. [2] proposed that some delamination and energy dissipation of the ceramic and UHMWPE composite armour during the ballistic test was due to the friction between the armour laminates or between the projectile and the armour laminates. Ong et al. [25] created a new composite armour which was composed of ceramic tile, Dyneema, porous foam plate and aluminium plate in sequence. Through the experimental work, they investigated the failure mechanisms of the constituent layers and energy absorption. Although this composite laminate concept was correct, they still needed to optimize the thickness of each layer to achieve a good ballistic performance with the minimum weight. Braga et al. [26] conducted series of high energy ballistic experiments on non-woven curaua fabric composites and aramid laminates. A hybrid composite panel was composed of a front layer of $Al_2O_3$ ceramic, a second layer of fabric or aramid, and a back layer of an aluminium alloy, the ballistic performance of curaua non-woven fabric composites was better than the aramid fabric (Kevlar) laminates.

Based on the review of the previous work, the research on the ballistic resistance of laminated composite structures is primarily focused on the ceramics combined with a metal or a reinforced fabric material. To date, there is limited work on the ballistic response of hybrid laminates consisted of ceramics, Dyneema, Kevlar and compressed wood. Therefore, the aim of the current paper is to investigate ballistic resistance of various hybrid laminated structures subjected to high velocity impact by a 7.62 mm incendiary projectile. Here, various hybrid laminated structures were first designed and fabricated. Then a series of ballistic impact tests were undertaken to investigate the ballistic response of those hybrid laminated structures made of combinations of silicon carbide or boron carbide, Dyneema, Kevlar and compressed wood. The ballistic impact tests were also carried out on panels made of a single material for comparison purpose and providing basic data for analytical models, which were developed to predict ballistic perforation performance of single material layers and the related hybrid composite structures. The perforation resistance and failure modes of the hybrid panels tested were assessed, together with the areal density. The outputs provide useful data for designing ballistic hybrid laminates.

# 2 Experimental procedure

## 2.1 Specimen preparation

The Kevlar fibre prepreg used in making hybrid ballistic panels was manufactured by the Dupont™ Company (Kevlar®). It is named Kevlar prepreg 2851HPP, which has a high performance proprietary PVB modified phenolic resin pre-impregnated rolled-goods. The yarn type is K129, with the thickness of 0.4 mm and the areal density of 450 g/m$^2$ per layer. The type of Dyneema ply was Dyneema® Unidirectional (UD) HB210, manufactured by DSM Company. It was made of UHMWPE that belongs to SK99 fibre type, with the density of 980 kg/m$^3$ and the layer thickness of 0.2 mm. The compressed wood was made of Scots pine.

The constituent materials of UHMWPE fibre and Kevlar fibre laminates as well as compressed wood panels were made separately using a hot press machine (Hare, UK) with a capacity of 200 tons and the temperature up to 400 °C. Both Kevlar and Dyneema laminates were produced following the manufacture processes provided by the suppliers, with recommended pressure cycles. There seems no common standard on producing various hybrid ballistic panels. For the Kevlar laminates, the curing pressure and temperature were 20 bars and 170 ºC, and the curing cycle remained for 15 minutes. For the Dyneema laminates, the curing pressure and temperature were 165 bars and 130 ºC, and the curing cycle remained for 40 minutes. As for the compressed wood, there were five steps during the hot-pressing procedure. The first step was pressure control, the curing pressure and temperature were 100 bars and 150 ºC remaining for 1 hour. Then, for the second to fifth steps, the curing pressure and temperature were 2000 bars and 150 ºC controlled by position. The position control of the height of each step was gradually decreased by 1/6 of the original panel thickness and kept for 5 minutes. At the end of the hot compressing on wood, the final thickness was 1/3 of its original thickness with a compressive ratio of 67 %. The press direction is along the radial direction of the wood.

Moreover, the silicon carbide (SiC) and boron carbide ($B_4C$) tiles were provided by Diamond Age Company. The plane dimensions of constituent panels are same as 100 mm×100 mm, with a thickness of 5 mm. All hybrid panels were fabricated by bonding constituent panels with epoxy resin (ET515 2-component structural adhesive, which has a good bond strength to a wide variety of substrates including metals and composites suitable for applications subject to vibration or shock) under room temperature for 24 hours, complying with the specific combinations as designed. Table 1 shows the six classifications of the fourteen types of hybrid panels, with the corresponding images being shown in Figure 1. Here, K, D, and T represent the abbreviation of Kevlar, Dyneema and compressed wood in Table 1.

Table 1. Hybrid composite laminate combinations in the sample preparation.

| Classification No. | Classification | Composition type |
|---|---|---|
| I | Ceramic + Fibre Reinforcement Material | 5mmSiC+10mmK |
| | | 5mmSiC+10mmD |
| | | 5mm$B_4C$+10mmK |
| | | 5mm$B_4C$+10mmD |
| II | Ceramic + Thin Compressed Wood + Fibre Reinforcement Material | 5mmSiC+2mmT+1.6mmK+3mmT+1.6mmK+1mmT+1.8mmD |

| | | |
|---|---|---|
| | | 5mm$B_4C$+2mmT+1.6mmK+3mmT+1.6mmK+1mmT+1.8mmD |
| III | Thick Compressed Wood + Thin Compressed Wood + Fibre Reinforcement Material | 5mmT+(2mmK+2mmT+2mmD)×5 |
| IV | Thick Compressed Wood + Fibre Reinforcement Material | 15mmT+5mmK+5mmD |
| V | Double Ceramic +Compressed Wood + Fibre Reinforcement Material | 5mmSiC+4.8mmT+5mm$B_4C$+2.25mmD |
| VI | Single plate of Ceramic, Fibre Reinforcement Material or Compressed Wood | 10mmSiC |
| | | 10mm$B_4C$ |
| | | 10mmK |
| | | 10mmD |
| | | 15mmT |

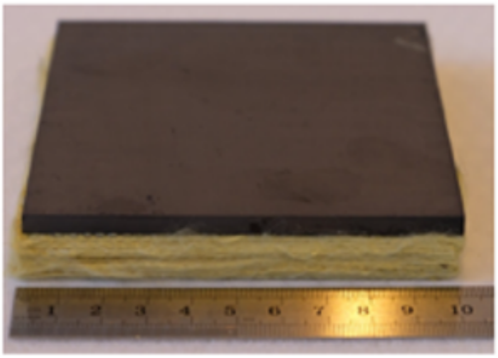

(a) Classification I

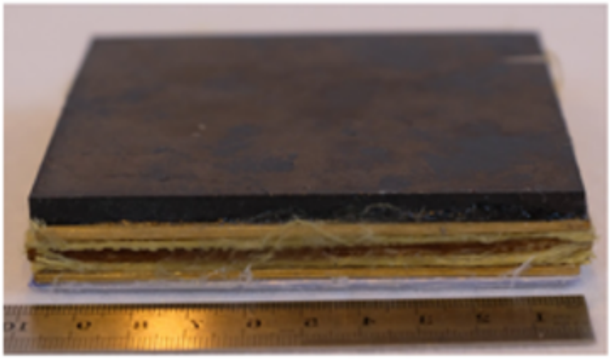

(b) Classification II

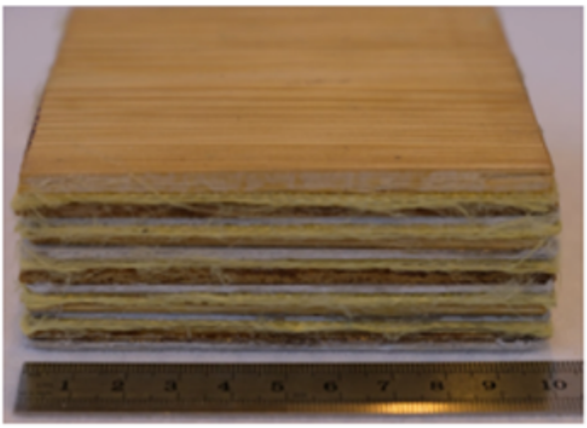

(c) Classification III

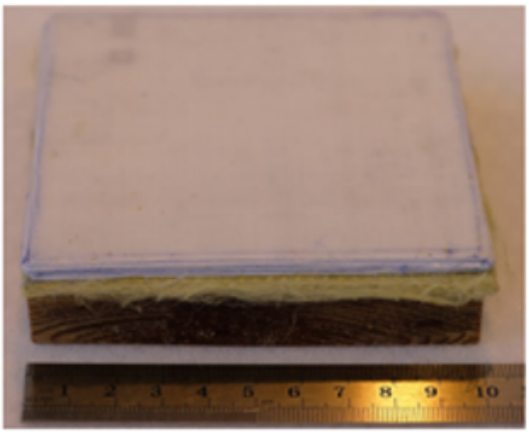

(d) Classification IV

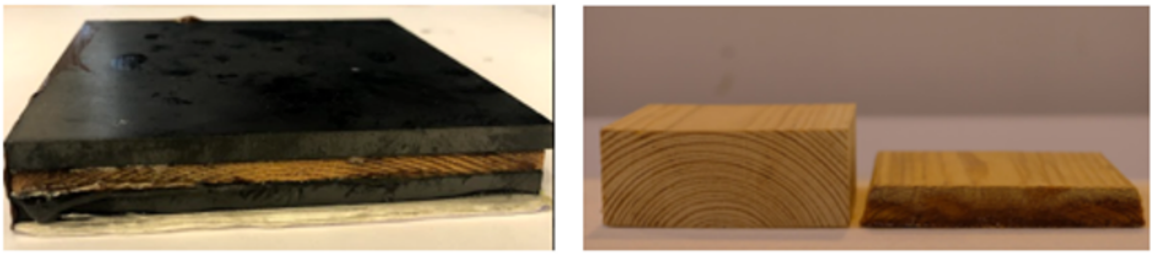

(e) Classification V (f) Classification VI

Figure 1. Images of five types of hybrid lamianted panels and single compressed wood panels.

## 2.2 Ballistic impact test

In the ballistic tests, a projectile of 7.62 × 39 mm (including hard steel core, lead filler and copper jacket) was launched by a normal ballistic rifle. A thin steel plate (150×150×2 $mm^3$) was attached to the back face of the target, to prevent the fabric to be pulled out of the fixture during the ballistic impact test. The initial projectile velocity before the penetration is defined as $V_i$ and the residual velocity after the full perforation as $V_r$. A high-speed camera (Phantom v2640) was used to record the dynamic deformation of the hybrid laminated structure during the penetration process in order to estimate $V_i$ and $V_r$. Figure 2 shows the schematic of the ballistic test setup, in which the projectile trajectory was perpendicular to the centre of the hybrid laminated target. Moreover, the bullet penetration location of all the targets were almost the same. Additionally, the initial velocity of the projectile was in the range from 806.0 to 887.5 m/s, due to the uncertainty of emission.

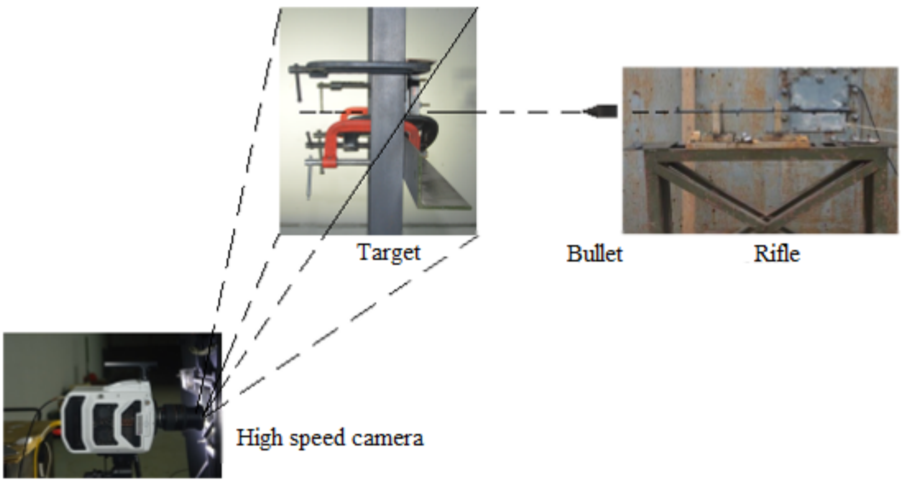


Figure 2. Schematic of ballistic test setting.

The geometry of the hybrid composite panel sample and the clamping device during the high-velocity impact tests are presented in Figure 3. As shown in Figure 3(a), the target panel was bonded to the middle of the 150 mm × 150 mm steel plate, which was acted as a rear support plate for the whole of structure. Eight M10 screws were used to clamp the target. Figures 3(a) and 3(b) show the front and the rear clamp plates with a square opening area of 70 mm × 70 mm at the centre. There were also four aluminium rectangular bars fixed around the composite panel to prevent the target from moving side way. The assembly drawing of the clamp with a target panel is illustrated in Figure 3(c), with the thickness of the front clamp, the steel rear plate, and the back clamp plate being 10, 2 and 8 mm, respectively. The thickness of the aluminium rectangular bar was slightly less than the thickness of the hybrid composite panels to ensure a tight clamping, which are 10, 15, 20, 25 and 38 mm for different hybrid panels, respectively. This could effectively protect the target panel in case it would fly out. Therefore, all the plates were screwed and tighten by the gaskets and the bolts at both sides.

(a)

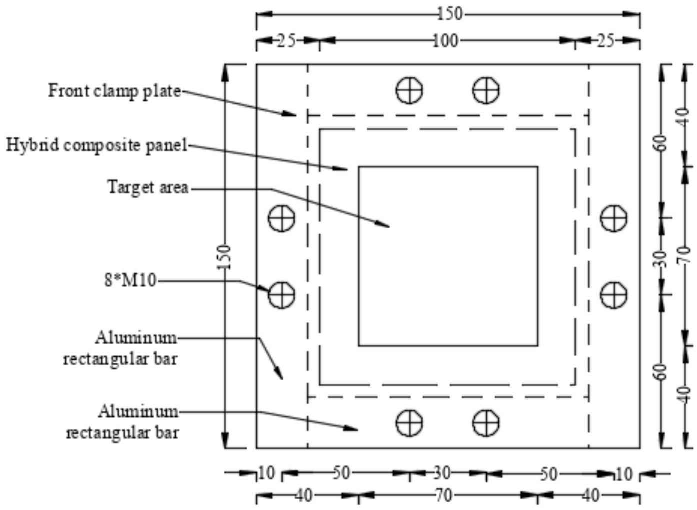


(b)

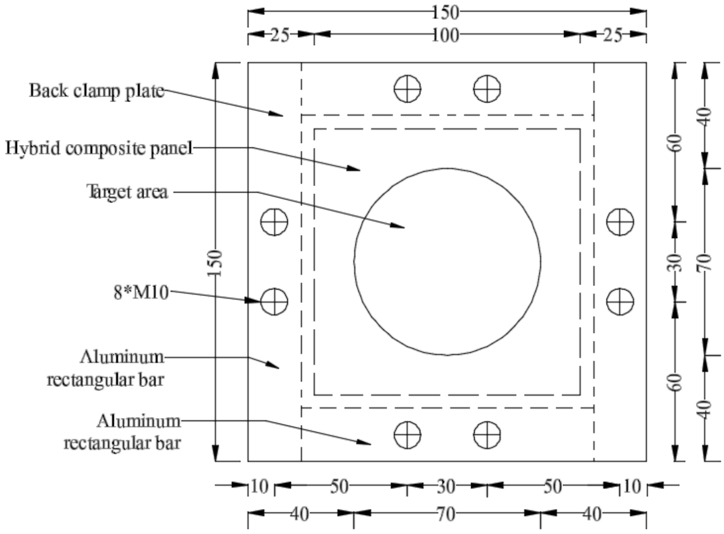


(c)

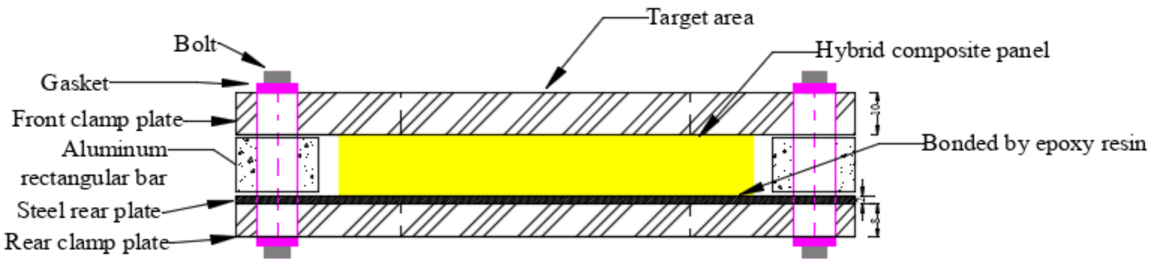


Figure 3. (a) geometry of the front steel clamp plate (b) geometry of the back steel clamp plate (c) schematic diagram of the assembled clamp with the hybrid composite panel (all dimensions in mm).

## 3 Predict perforation behaviour of different material layers by a bullet

Analytical models are developed to predict ballistic resistance of a single material layer and the related hybrid panels. As the penetration process of a bullet through ceramic and steel has been widely studied, the analytical models of these materials have been simplified and expressed in a uniformed formula. However, the failure of plain-woven fabric layer varies at different impact velocities and has a significant influence on the final perforation. Therefore, the deformation of plain-woven fabric layer during penetration by a bullet is a crucial problem to be dealt in the current paper. An idealised model of a composite structure penetrated by a bullet is proposed in Fig. 4, with assumptions being made as follows:

(1) Core of bullet is perfectly rigid,

(2) The damage evolution in ceramic is ignored,

(3) Longitudinal and transverse wave velocities are the same in all the layers of plain-woven target,

(4) Friction between the bullet and the composite is neglected.

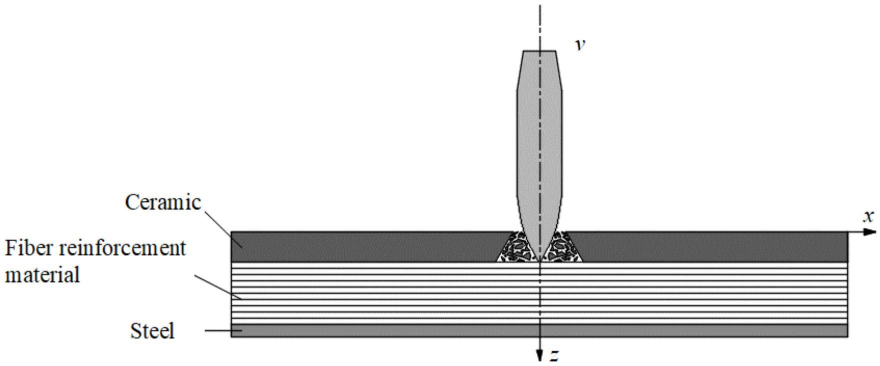


Fig. 4. The model of a composite structure penetrated by a bullet

**3.1 Ceramic and steel**

It was observed through the experiments that the residual velocity of bullet after perforation of a composite plain weave layer (either Kevlar or Dyneema) is high enough to perforate the thin steel back plate. There is a further velocity decay after a bullet perforates the steel, which is attributed to the work of resistant force offered by the steel back plate. The principle of velocity decay of a bullet in the perforation of a single ceramic or compressed wood plate can be regarded as the same as that of a bullet in perforation of steel. The residual velocity of a bullet after the perforation of ceramic, steel or compressed wood can be written as

$$v_r = \sqrt{v_i^2 - \frac{2\sigma_t A_p h}{m_p}} \quad (1)$$

where $\sigma_t$ is the resistance of target, $A_p$ is the cross-sectional area of projectile, $h$ is the thickness of target, $v_i$ and $v_r$ are impact velocity and residual velocity of a bullet, $m_p$ is the mass of bullet, respectively.

3.2 **Fibre reinforced materials**

During the penetration of a 7.62mm bullet through woven fabric composite, the initial kinetic energy is absorbed by the kinetic energy of moving cone ($E_{KE}$), shear plugging ($E_{SP}$), the deformation of secondary yarns ($E_D$), tensile failure of primary yarns ($E_{TF}$), delamination ($E_{DL}$), matrix cracking ($E_{MC}$) and energy absorbed by friction ($E_F$) [27].

According to the failure mode observed in the experiment, neither the shear plugging of the composite layer nor that of steel plate occur during the perforation. Therefore, the energy absorbed due to shear plugging is taken as zero.

The cone formation and the damage propagation in the composite during ballistic impact are shown in Fig. 5. $r_{pi}$ refers to the distance covered by the plastic wave till time t.

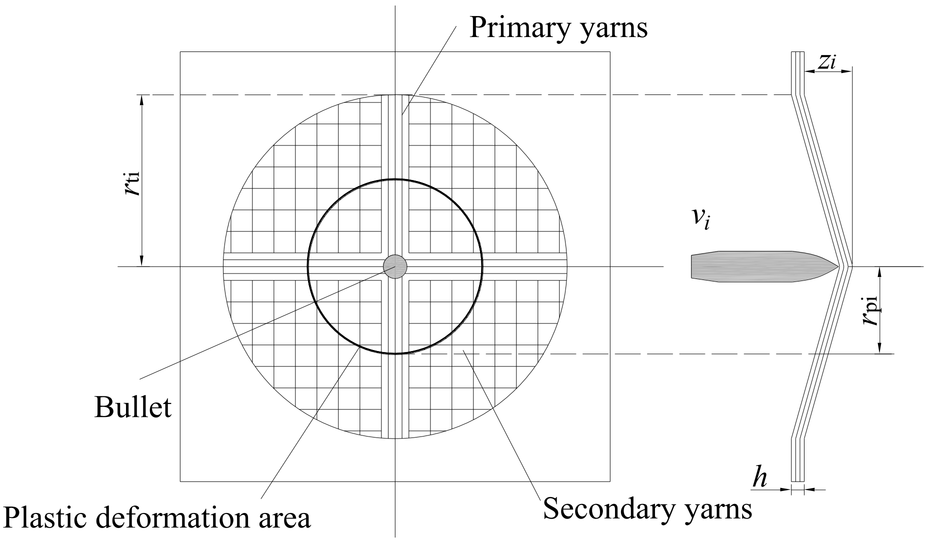


Fig. 5. Cone formation in woven fabric composite during ballistic impact [27]

The strain is generated instantaneously in yarn when the bullet impacts the target, which can be obtained through the following equation [28].

$$v = \sqrt{\frac{E}{\rho}(2\varepsilon\sqrt{\varepsilon(1+\varepsilon)} - \varepsilon^2)} \quad (2)$$

where $v$ is the impact velocity of bullet, $E$ is Young's modulus of yarn, $\rho$ is volume density of yarn and ε is strain.

The transverse wave velocity at the base of the cone (Fig. 5) to spread is

$$c_t = \left(\sqrt{(1+\varepsilon)\varepsilon} - \varepsilon\right)\sqrt{\frac{E}{\rho}} \quad (3)$$

The plastic wave propagates at a velocity of

$$c_p = \sqrt{\frac{1}{\rho}\left(\frac{\mathrm{d}\sigma}{\mathrm{d}\varepsilon}\right)_{\varepsilon=\varepsilon_p}} \tag{4}$$

Assuming that $t_i = i\Delta t$, the radius $r_{ti}$ and $r_{pi}$ (Fig. 5) can be written as

$$r_{ti} = \sum_{n=0}^{i} c_{tn} \Delta t \tag{5}$$

$$r_{pi} = \sum_{n=0}^{i} c_{pn} \Delta t \tag{6}$$

Strain at the point of impact is given by

$$\varepsilon_i = \left\{ \frac{d/2 + \sqrt{(r_{ti} - d/2)^2 + z_i^2} + \left(r_{pi} - r_{ti}\right) - r_{pi}}{b^{r_{pi}/\mathrm{a}} - 1} \right\} \left( \frac{\ln \mathrm{b}}{a} \right) \tag{7}$$

where $a$ is the yarn width, $d$ is the projectile diameter, $b$ is the stress wave transmission factor, $z_i$ is the height of the cone, which equals to the distance traveled by the projectile.

$$v_{ri} = \sqrt{\frac{\frac{1}{2} m_p v_i^2 - E_{i-1}}{\frac{1}{2} m_p}} \tag{8}$$

$$E_{i-1} = E_D + E_{TF} + E_{DL} + E_{MC} \tag{9}$$

$$z_i = \sum_{n=0}^{i} \left[ v_{i-1} \Delta t + \frac{1}{2} \frac{v_{i-1} - v_i}{\Delta t} \left( \Delta t \right)^2 \right] \tag{10}$$

The force of projectile acts on the surface of the woven fabrics is

$$F_i = m_p \frac{v_{i-1} - v_i}{\Delta t} \tag{11}$$

The secondary yarns experience different strains from A to B (Fig. 5). At the centre point (impact location), the strain of the secondary yarn is equal to the primary yarn, while at the fixed boundary, the strain is 0. Thus, the strain can be expressed as

$$\varepsilon_{\mathrm{sy}} = \frac{\left(r_{ti} - r\right)\varepsilon_{py}}{r_{ti} - \frac{d}{2}} \left(\frac{d}{2} < r < r_{ti}\right) \tag{12}$$

where $\varepsilon_{\mathrm{py}}$ is the strain at the outermost primary yarn in that layer. The energy absorbed in the formation of all the secondary yarns can be then obtained.

$$E_{Di} = h\int_{d/\sqrt{2}}^{r_{ti}} \left[ \int_0^{\varepsilon_{syi}} \sigma_{sy}\left(\varepsilon_{sy}\right) \mathrm{d}\varepsilon_{sy} \right] \left[ 2\pi r - 8r\sin^{-1}\left(d/2r\right) \right] \mathrm{d}r \tag{13}$$

The energy absorbed by the tensile failure of the primary yarn is written as

$$E_{TFi} = NA\int_o^x \left( \int_{\varepsilon=0}^{\varepsilon=\varepsilon_0 b^{x/a}} \sigma\left(\varepsilon\right) \mathrm{d}\varepsilon \right) \mathrm{d}x \tag{14}$$

where $N$ is the number of yarns failed, $A$ is the cross-section area of yarn, $\varepsilon_0$ is the maximum strain in a yarn.

The energy absorbed by the delamination and matrix cracking are written as

$$E_{DLi} = \sum_{n=1}^{i} P_d \pi (r_{di}^2 - r_{d(\mathrm{i}-1)}^2) A_{ql} G_{IIcd} \tag{15}$$

where $A_{\mathrm{ql}}$ is the quasi-lemniscate reduction factor, $G_{\mathrm{IIcd}}$ is the critical dynamic strain energy release rate at mode II (the interlaminar strength of the composite decreases due to matrix cracking, with the delamination being resulted from further loading and deformation), $P_{\mathrm{d}}$ is the percentage of delaminating layers. Furthermore, there is

$$E_{MCi} = \sum_{n=1}^{i} P_{\mathrm{m}} \pi (r_{di}^2 - r_{d(i-1)}^2)\, A_{ql} E_{mt} h \tag{16}$$

where $P_{\mathrm{m}}$ is the percentage of matrix cracking, $E_{\mathrm{mt}}$ is energy absorbed by matrix cracking per unit volume.

There are likely different modes of perforation by a bullet. At a high impact velocity (higher than $\sqrt{\frac{E}{\rho}(2\varepsilon_0\sqrt{\varepsilon_0(1+\varepsilon_0)}-\varepsilon_0^2)}$) the strain exceeds the maximum strain and yarn suffers tensile failure at the instance of impact with negligible deformation at failure. The energy absorbed by the fibre is composed of tensile failure of primary yarns ($E_{TF}$), delamination ($E_{DL}$) and matrix cracking ($E_{MC}$). At a low impact velocity, the bullet pushes the fibre to form a cone, the kinetic energy of bullet is consumed by the deformation of secondary yarns ($E_D$). The yarn cannot be prolonged when the strain in yarn reaches the maximum strain. According to the boundary conditions, the maximum distance of a bullet, $d_b$, without penetrating yarn can be written as,

$$d_b = B\sqrt{(1+\varepsilon_0)^2-1} \quad (17)$$

where B is the radius of the yarn being constrained.

When a bullet is not stopped by the energy absorption due to deformation of secondary yarns, the bullet begins to perforate the yarn. For the analysis of a bullet perforation through woven fabric composites, the deformation of secondary yarns should be included.

# 4 Results and discussion

## 4.1 Perforation of the hybrid panels subjected to the high-velocity impact

From the high-velocity impact tests, it was observed that some of the composite panels were partially penetrated, and the others were fully perforated. The kinetic energy absorbed ( $E_{abs}$ ) by the different composite panels during the high-velocity impact tests can be given as:

$$E_{abs} = \frac{1}{2}mV_i^2 - \frac{1}{2}mV_r^2 \quad (18)$$

where m is the mass of the 7.62 mm projectile, $V_i$ is the initial striking velocity, $V_r$ is the residual velocity. The mass loss of the bullet is neglected. Although the core is deformed, it still attaches to the jacket. Therefore, the failure of bullet is assumed not to cause significant loss of the bullet mass.

The results of high-velocity impact tests for all composite panels are illustrated in Table 2, which includes areal density, initial and residual velocity, energy absorption and constituent materials. Except for sample C1 (armor piercing), all other tests used 7.62 mm projectile.

Table 2. Ballistic test results of all composite panels.

| Composite Panel | Back steel plate | Sample No. | Areal density ($kg/m^2$) | Actual thickness (mm) | Initial velocity ($v_i$)(m/s) | Residual velocity ($v_r$)(m/s) | Energy absorption ($E_{abs}$, J) | Failure mode |
|---|---|---|---|---|---|---|---|---|
| 5mmSiC+10mmK | Yes | A1 | 28.02 | 15.28 | 825.00 | 201.00 | 3431.6 | FP |
| 5mmSiC+10mmK | Yes | A2 | 28.28 | 15.27 | 825.43 | 124.98 | 3568.2 | FP |
| 5mmSiC+10mmD | Yes | A3 | 25.17 | 14.02 | 812.00 | 0 | 3534.1 | PP |
| 5mmSiC+10mmD | Yes | A4 | 25.14 | 14.40 | 836.25 | 0 | 3748.3 | PP |
| 5mmSiC+10mmD | Yes | A5 | 25.18 | 14.67 | 840.50 | 0 | 3786.5 | PP |
| 5mm$B_4C$+10mmK | Yes | A6 | 24.56 | 15.33 | 835.82 | 161.69 | 3604.3 | FP |
| 5mm$B_4C$+10mmK | Yes | A7 | 24.43 | 15.08 | 833.64 | 397.03 | 2880.1 | FP |
| 5mm$B_4C$+10mmK | Yes | A8 | 24.54 | 15.11 | 836.17 | 45.90 | 3736.3 | FP |
| 5mm$B_4C$+10mmD | Yes | A9 | 21.54 | 13.72 | 827.27 | 0 | 3668.3 | PP |
| 5mmSiC+2mmT+1.6mmK+3mmT+1.6mmK+1mmT+1.8mmD | Yes | B1 | 29.54 | 17.20 | 821.89 | 293.23 | 3159.8 | FP |
| 5mmSiC+2mmT+1.6mmK+3mmT+1.6mmK+1mmT+1.8mmD | Yes | B2 | 30.11 | 17.57 | 830.32 | 431.74 | 2696.3 | FP |
| 5mm$B_4C$+2mmT+1.6mmK+3mmT+1.6mmK+1mmT+1.8mmD | Yes | B3 | 27.83 | 17.49 | 831.93 | 477.98 | 2485.1 | FP |
| 5mm$B_4C$+2mmT+1.6mmK+3mmT+1.6mmK+1mmT+1.8mmD | Yes | B4 | 27.64 | 18.27 | 840.36 | 366.29 | 3066.1 | FP |
| 5mm$B_4C$+2mmT+1.6mmK+3mmT+1.6mmK+1mmT+1.8mmD | Yes | B5 | 26.31 | 18.73 | 846.61 | 489.57 | 2557.1 | FP |
| 5mmT+(2mmK+2mmT+2mmD)×5 | Yes | C1 | 43.11 | 37.92 | 832.21 | 668.54 | 1316.6 | FP |
| 5mmT+(2mmK+2mmT+2mmD)×5 | Yes | C2 | 43.40 | 38.53 | 822.13 | 644.30 | 1397.8 | FP |
| 15mmT+5mmK+5mmD | Yes | D1 | 29.51 | 25.11 | 836.63 | 665.50 | 1377.8 | FP |

| | | | | | | | | |
|---|---|---|---|---|---|---|---|---|
| 15mmT+5mmK+5mmD | Yes | D2 | 28.53 | 24.65 | 839.63 | 716.62 | 1026.1 | FP |
| 5mmSiC+4.8mmT+5mmB$_4$C+2.25mmD | Yes | E1 | 38.50 | 17.74 | 838.20 | 0 | 3765.8 | PP |
| 10mmSiC | None | F1 | 33.40 | 10.49 | 814.00 | 490.35 | 2262.7 | FP |
| 10mmB$_4$C | Yes | F2 | 26.10 | 10.42 | 829.88 | 229.74 | 3408.5 | FP |
| 10mmK | Yes | F3 | 11.50 | 9.93 | 826.56 | 749.73 | 649.1 | FP |
| 10mmD | Yes | F4 | 8.50 | 8.53 | 836.90 | 767.45 | 597.2 | FP |
| 15mmT | None | F5 | 17.90 | 15.00 | 887.50 | 862.50 | 234.5 | FP |
| 15mmT | None | F6 | 18.90 | 14.90 | 806.00 | 720.00 | 703.4 | FP |

PP: partial penetration; FP: full perforation

Most of hybrid panels were bonded with a thin steel plate at the back side, which was used to accommodate the back face fabrics peeled off. However, the values of the areal density for these panels do not include the thin steel back plate. The areal density of the targets is in a range from 17.90 to 43.40 kg/m$^2$, and their actual thickness is from 8.53 to 38.53 mm. As mentioned before, the initial velocity was varied from 806.0 to 887.5 m/s. However, the residual velocity was in a range from 0 m/s (no perforation) to 862.5m/s (fully perforated). There were five panels which successfully resist the bullet, i.e. partial penetration (PP), and the rest of twenty panels were with full perforation (FP). For samples A1-A9, they consisted of 5 mm ceramic (SiC or B$_4$C) front plate, 10 mm fabric laminates (Dyneema or Kevlar) and 2 mm steel back plate. It was found that the SiC and B$_4$C tiles with Dyneema (A3-A5 and A9) could resist the ballistic impact. The panel A9 made of B$_4$C tile and Dyneema and steel back plate has the lowest areal density (21.54 kg/m$^2$) with an overall thickness of 13.72 mm, among the four partial penetration panels. However, the panels made of SiC or B$_4$C and Kevlar (A1, A2, and A6 - A8) were perforated, with various residual velocity from 46 to 397 m/s. It is surprised that there are largely scattered residual velocities for 5 mm B$_4$C and 10 mm Kevlar panels.

The samples B1- B5, which were made of ceramic SiC or B$_4$C tile with multiple thin compressed wood (CW) and fabric laminates (Table 2), were fully perforated, with residual velocities in a range from 293 and 490 m/s. Such the combinations of SiC or B$_4$C, CW and Kevlar or Dyneema seem not effective. It is understandable that the areal density of the SiC based panels (B1 and B2) is higher than the B$_4$C based panels (B3, B4 and B5), due to the higher density of SiC. The energy absorptions of those panels are related to the corresponding residual velocities. Regarding to CW based panels with thin Kevlar and Dyneema laminates (C1 and C2), they are relatively easily perforated by both the 7.62mm Armor-piercing incendiary projectile and 7.62 mm ordinary projectile, with large residual velocities of 669 and 644 m/s. The energy absorption of C2 was slightly higher than C1, as the projectile of the former is more powerful than the latter However, the sensitivity of the projectile type to this kind of panel is low.

The panels D1 and D2, fabricated with a thick compressed wood (10 mm) and thick fabric laminates (5 mm Kevlar and 5 mm Dyneema), do not show a good resistance to ballistic impact, with a high residual velocity of 717 m/s. The front face of type C and type D panels was compressed wood without any ceramic tiles, which is not effective. Therefore, it is crucial to have a ceramic front layer to blunt the bullet before it enters the fibre reinforced composite. Type A panels not only have much lower areal density and thickness than Type C panels, but also their energy absorption are three times of that of the latter.

Panel E1 (Table 2), which is made of both SiC and $B_4C$ tiles with compressed wood and Dyneema fabric laminates, resists the bullet successfully. The thickness of panel E1 is only half of that of panel C2, but with relatively high areal density in comparison to type A, B and D panels. Finally, type F panels made of a single material demonstrate various ballistic resistances. It clearly shows that the residual velocities of the Kevlar panel (F3), Dyneema panel (F4) and CW panels (F5 and F6) are much higher than that of both ceramic targets (F1 and F2). This again indicates the importance of the ceramic layer placed in the front. Otherwise, much thicker fibre reinforced composite are needed to resist the bullet.

Figs. 6 and 7 show the relationship between areal density and energy absorption and residual velocity of all the hybrid and single material panels tested, respectively. As expected, relatively thin single material panels, i.e. type F, have the lowest areal density and energy absorption and highest residual velocity, except for ceramic panels. The SiC panel (F1) has a higher areal density than the $B_4C$ tile (F2) with a thin steel back plate. As a result, the $B_4C$ panel absorbed more energy with lower residual velocity than the SiC one. Among type A, B and D panels with moderate areal density, type

A panels have the better performance than other types, especially for panel A9 (5 mm $B_4C$, 10 mm Dyneema) which has the lowest areal density, thickness and relatively high energy absorption (Fig. 6) and zero residual velocity (Fig. 7). In addition, the panels made of 5 mm $B_4C$ and 10 mm Kevlar also show a reasonably good performance with relatively low areal density, residual velocity and high energy absorption. As for the type B panels, although $B_4C$ front plate has slightly lower areal density than SiC one, the average energy absorption of the $B_4C$ based hybrid panels (B3, B4 and B5) is in fact lower than that of the SiC based ones (B1 and B2, Fig. 6). As a result, the average residual velocity of the $B_4C$ hybrid panels is slightly higher than that of the SiC based ones (B1 and B2, Fig. 7). This may be attributed to the lamination combinations, in which SiC layer seems working well with other materials lamination. Regarding type D and type C panels, they both have compressed wood constituent plates. Type D panels have a 15 mm thick compressed wood front plate, whilst type C panels have a 5 mm thick compressed wood front plate, followed by five thin compressed wood plates (each thickness=2 mm) combined with fabric (Kevlar and Dyneema) laminates. The areal density of type D is approximately 25 % lower than type C type panels. However, the average energy absorption and residual velocity of the latter are only increased and decreased by 12 % and 5 % in comparison to the former, respectively.

Although type E panel has a high energy absorption value and zero residual velocity, the corresponding areal density is also high, due to using two 5 mm ceramic tiles in the panel. Based on the experimental investigations of panel G1 by Nguyen et al. [29] shown in Fig. 7, G1 is a 100 mm × 100 mm × 10 mm Dyneema target (areal density = 9.8 kg/m$^2$) and perforated by a 20 mm FSP projectile. The initial velocity is 836 m/s, and the residual velocity is 762 m/s. The areal density of the panel G1 is approximately 15% higher than the panel F4. However, the average residual velocity of the panel G1 is almost same as that of F4. Furthermore, the panel G2 [12], fabricated with nine mosaic thick SiC tiles (8 mm) and thick fabric laminates (8 mm Dyneema), with a high areal density of 33.56 kg/m$^2$ also a high residual velocity of 100 m/s. Compared to the panels A3 - A5, not only the panel G2 has higher areal density, but also it has higher residual velocity.

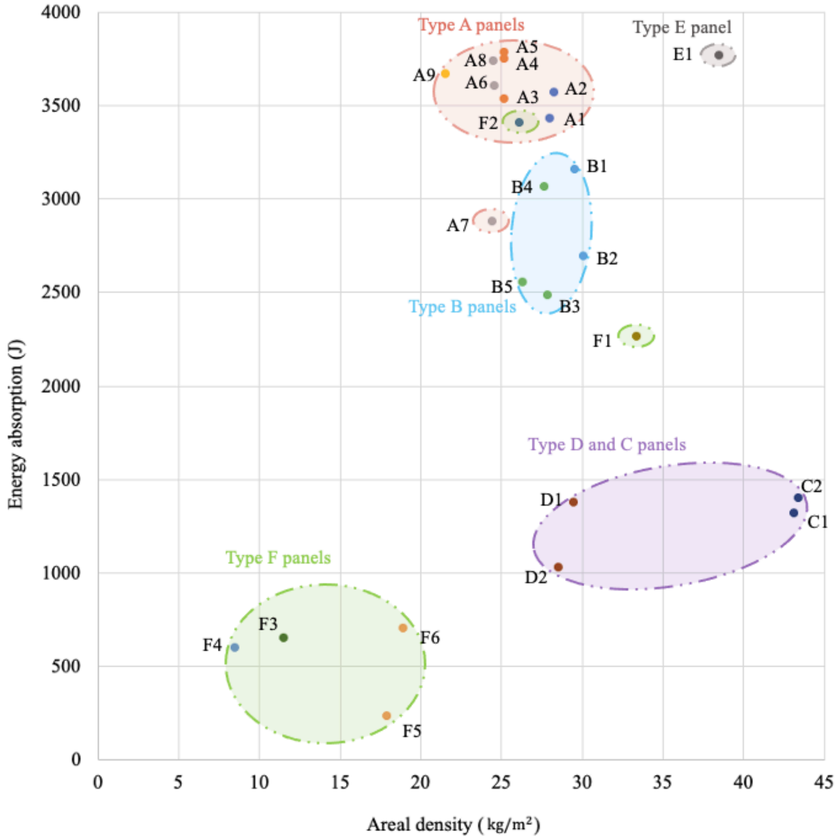


Figure 6. Relationship between areal density and energy absorption of different panels.

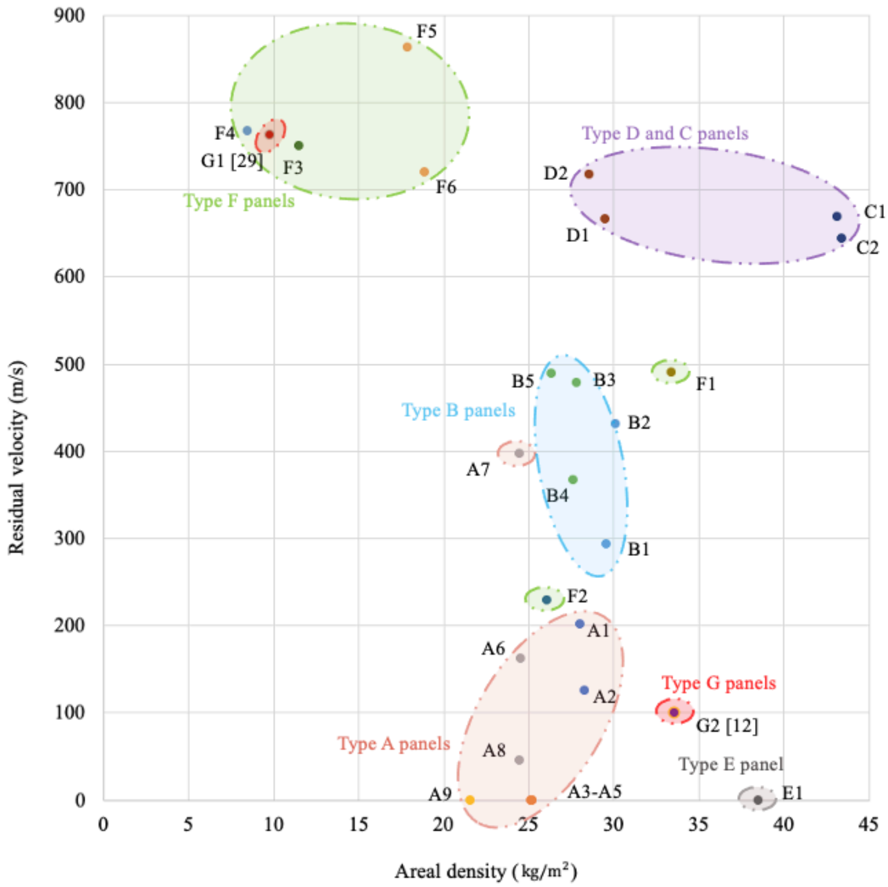

Figure 7. Relationship between areal density and residual velocity of different panels.

### 4.2 Failure mode of the hybrid panels subjected to the high-velocity impact

After the ballistic tests, the bulging deformations (or signatures) of the hybrid laminated panels were measured. The schematic diagrams for measuring $h_1$, $h_2$ and $h_3$ are shown in Fig. 8, together with failure modes for panels A3 and A4. There are two cases of the bulged back steel plate, i.e. (1) no splitting damage (Fig.8a), (2) partial edge tearing (Fig. 8b). The maximum bulging deformation from the position of the undeformed steel plate to the peak point of the doom is defined as $h_1$ (Fig. 8c), the maximum bulging deformation from the bulged fabric to the undeformed steel plate as $h_2$ (Fig. 8d) and the maximum crater depth as $h_3$ (Fig. 8c), which are listed in Table 4 for panels with such the measurements. As shown in Fig. 8(c), if the back steel plate is not perforated, i.e. the hybrid panel is partially penetrated by the projectile, the bulging deformation from the steel ($h_1$) and the maximum crater depth ($h_3$) can be measured. If the hybrid target is fully penetrated, $h_3$ cannot be measured. However, in the partial damaged back steel plate shown in Fig. 8(d), if the fabric layer is partially penetrated, the bulging deformation from the steel ($h_1$), the bulging deformation from the fabric ($h_2$) and the maximum crater depth ($h_3$) can be measured. If the target is perforated, together with the steel plate, it is only necessary to measure $h_1$ and $h_2$.

(a) (b)

(c)

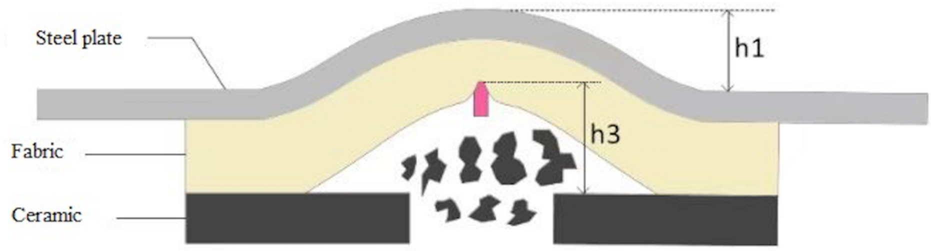


(d)

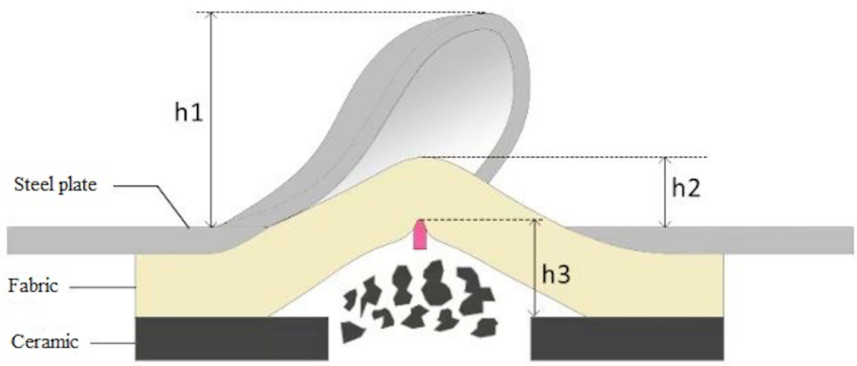


Figure 8. Failure modes: (a) image of composite panel A3 after the ballistic test (b) image of composite panel A4 after the ballistic test (c) schematic diagram for measuring the bulging deformation on the non-perforated back steel plate (d) schematic diagram for measuring the bulging deformation on the partially tearing steel plate.

As shown in Table 3, for all panels with full perforation, only the back steel plates on panels A1, A3, B5, F3 and F4 were not separated from the fabric layer, i.e. the steel plate was still covering the fibre reinforced composite layer. Therefore, it is difficult to observe the residual deformation mode of the fabric layer and to tell how the perforation process affect the bulging pattern of the back steel plate, as cutting through the central cross-section of the panels will certainly alter the deformation mode. For panels A4 to A9, the back steel plate was partially split from the hybrid panels, and the maximum and minimum bulging deformations of the steel plate were 52.5 mm (panel A8) and 21.8 mm (panel A7), respectively. Both the back steel plates of targets A1 and A3 were not split, with $h_1$ (21.8 mm) of A1 being slightly greater than that of A3 (20.5 mm). Then, $h_2$ of panels

A4, A5 and A9 (partial penetration case) were higher than that of panels A6 - A8 (full perforation). Also, panel A5 absorbed the highest energy, associated with the largest $h_2$. However, panels A6 - A8 were fully perforated by the projectile and the permanent bulging deformations of the fabric layer ($h_2$) were lower than that of the partially penetrated panels, due to the more recovered deformations. Moreover, for the hybrid laminated panels (5 mm ceramic, 10 mm Dyneema with 2 mm steel back plate), it was found that the maximum crater depth ($h_3$) was increasing with the growth of the energy absorption of the panels with partial penetration (A3 - A5 and A9). Moreover, $h_3$ of panel E1 was only 12.2 mm, which was less than the above four panels, although the energy absorption of E1 was also close to theirs. This was because the bulging deformation of the ceramic or compressed wood laminates was negligible, but the original thickness of fabric laminate was only 2.3 mm. Therefore, the value of the maximum crater depth ($h_3$) was primarily influenced by the thickness of the fabric laminates.

In type B panels, panel B1 shows the highest energy absorption, but its permanent displacement on the back face, $h_1$, is relatively low. In fact, the difference on $h_1$ of type B panels in comparison to the average value is less than 20 %, with three panels (B1-B3) being close to the averaged $h_1$, as the design of the hybrid laminates is similar. The back face signature, i.e. bulging deformations of the back steel plate ($h_1$), is closely related to energy absorption, for these ceramic, thin fabric and compressed wood laminated hybrid panels. Compared panel C2 with panels D1 and D2, the back steel plate of C2 was not split at the clamping boundary, with its permanent displacement, $h_1$, being equal to 15.6 mm, which is much higher than the permanent displacement $h_2$ of the back fabric layer of panels D1 and D2 (6.78 and 2.02 mm). This is partially due to the total fabric laminate thickness of type C panel (fabric thickness=20 mm) being twice of type D panel (fabric thickness=10 mm), and partially non-edge failure of the back steel plate. Panels D1 and D2 were both composed of a thick compressed wood with thick fabric laminates, closed by a thin steel plate. In terms of type F panels (Table 3), the deformations of the panels with ceramic tiles and CW plate were negligible. The Dyneema panel (F4) has a bigger bugling deformation ($h_1$ = 14.20 mm) compared to that (10.14 mm) of the Kevlar one (F3) with a similar thickness, as the former has more stretchable ability than the latter.

Table 3. Bulging deformations of all panels tested.

| Hybrid Panel | Panel No. | Bulging deformation from Steel $h_1$ (mm) | Bulging deformation from fabric $h_2$ (mm) | Maximum crater depth $h_3$ (mm) |
|---|---|---|---|---|
| 5mmSiC+10mmK | A1 | 21.82 | N. A | N. A |
| 5mmSiC+10mmD | A3 | 20.52 | N. A | 19.82 |
| 5mmSiC+10mmD | A4 | 44.70* | 20.53 | 21.06 |
| 5mmSiC+10mmD | A5 | 34.06 | 21.78 | 25.48 |
| 5mm$B_4C$+10mmK | A6 | 31.35 | 14.38 | N. A |
| 5mm$B_4C$+10mmK | A7 | 21.75 | 10.35 | N. A |
| 5mm$B_4C$+10mmK | A8 | 52.46* | 10.06 | N. A |
| 5mm$B_4C$+10mmD | A9 | 26.14 | 14.56 | 20.66 |
| 5mmSiC+2mmT+1.6mmK+3mmT+1.6mmK+1mmT+1.8mmD | B1 | 23.21 | N. A | N. A |
| 5mmSiC+2mmT+1.6mmK+3mmT+1.6mmK+1mmT+1.8mmD | B2 | 23.56 | N. A | N. A |
| 5mmB4C+2mmT+1.6mmK+3mmT+1.6mmK+1mmT+1.8mmD | B3 | 23.50 | N. A | N. A |
| 5mm$B_4C$+2mmT+1.6mmK+3mmT+1.6mmK+1mmT+1.8mmD | B4 | 28.17 | N. A | N. A |
| 5mmB4C+2mmT+1.6mmK+3mmT+1.6mmK+1mmT+1.8mmD | B5 | 18.87 | N. A | N. A |
| 5mmT+(2mmK+2mmT+2mmD)×5 | C2 | 15.60 | N. A | N. A |
| 15mmT+5mmK+5mmD | D1 | 28.05 | 6.78 | N. A |
| 15mmT+5mmK+5mmD | D2 | 12.16 | 2.02 | N. A |
| 5mmSiC+4.8mmT+5mm$B_4C$+2.25mmD | E1 | 32.36 | N. A | 12.16 |
| 10mmK | F3 | 10.14 | N. A | N. A |
| 10mmD | F4 | 14.20 | N. A | N. A |

*Fail to meet NIJ standard 0101.06 [30]

The typical failure modes of type A panels after ballistic impact tests are shown in Figs. 9 - 12 (A1, A4, A6 and A9). Both SiC and $B_4C$ ceramic front tiles were completely smashed into many small fragments along radial cracks originated from the striking location after the bullet struck and penetrate them. However, as the back fabric layer was Dyneema for panels A4 and A9, more fragments were remained in the panel for both types of ceramic front plates (Figs. 10 and 12), in comparison to panels A1 and A6 (Figs. 9 and 11). This is because Dyneema fabric has a higher out-of-plane Young's modulus than Kevlar fabric, so that it can provide sufficient support to the ceramic tile, reduce bending deformation, as well as delay the occurrence of tensile fracturing of the ceramic tile. The back steel plates for panels A1 and A6 were perforated with a typical ductile failure mode of a metallic material (Figs. 9 and 11). The back steel plate of panel A1 is still partially bonded to the Kevlar fibric layer after the ballistic test, however the back steel plate of panel A6 was torn apart from the clamping boundary. Therefore, it can be observed from Fig. 10 that there were two slight draw-in of the Kevlar layer at the clamping edge due to the large bulge deformation during test, and the bullet hole was closed by the surrounded Kevlar fibres. Both panels A4 and A9 were partial penetrated, with the corresponding bulge deformations being clearly seen in the diagram. Panel A9 shows more drawn-in of Dyneema than A4, even the former had delamination between ceramic tile and Dyneema laminate.

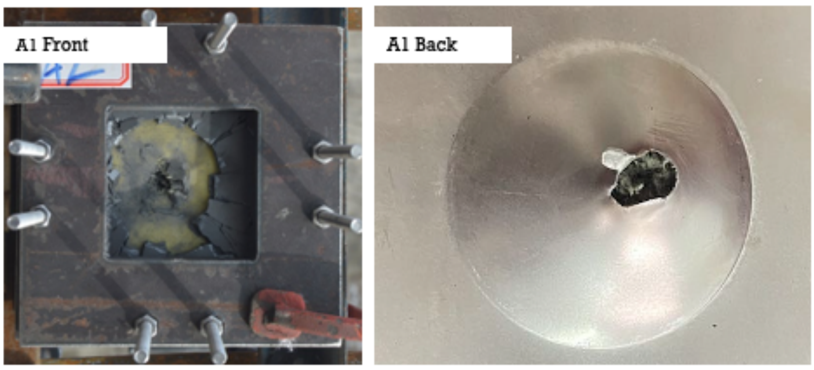


Fig. 9. Failure mode of panel A1 (5 mm SiC + 10 mm Kevlar + 2 mm back steel plate): the front face (left) and back face (right).

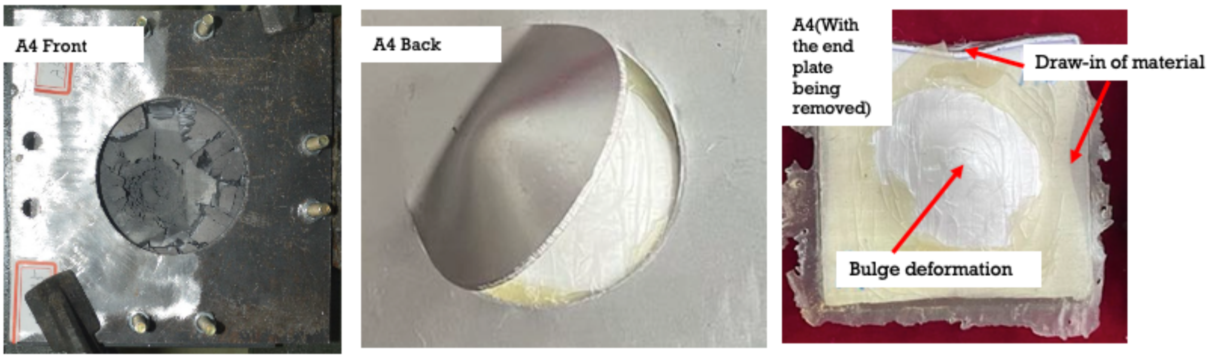


Fig. 10. Failure mode of panel A4 (5 mm SiC + 10 mm Dyneema with a 2 mm steel plate): the front face (left), back face (middle) and with back plate being removed (right).


Fig. 11. Failure mode of panel A6 (5 mm $B_4C$ + 10 mm Kevlar with a 2 mm steel plate): the front face (left), back face (middle) and with back plate being removed (right).


Fig. 12. Failure mode of panel A9 (5 mm $B_4C$ + 10 mm Dyneema with a 2 mm steel plate): the front face (left), back face (middle) and with back plate being removed (right).

In terms of type B panels, the only difference of them is the ceramic material on the front face, i.e. SiC or $B_4C$. The failure modes of both types of panels are similar, as presented in Figs. 13 and 14. Both the ceramic tiles were fragmented after bullet struck, and the back steel plates were perforated with a bulge deformation, showing a ductile failure mode. The bullet holes on the back Dyneema material of both B2 and B4 panels could be clearly seen. There were also some drawn-in of Dyneema material (Figs. 13 and 14).


Fig. 13. Failure mode of B2 (5 mm SiC + 6 mm compressed wood + 5 mm fabric laminates in total with a 2 mm steel plate): the front face (left), back face (middle) and with back plate being removed (right).

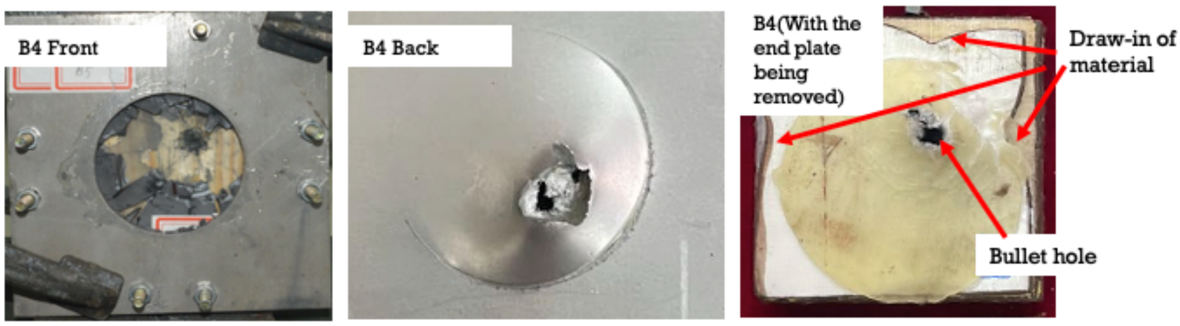


Fig. 14. Failure mode of B4 (5 mm $B_4C$ + 6 mm compressed wood + 5 mm fabric laminates in total with a 2 mm steel plate): the front face (left), back face (middle) and with back plate being removed (right).

On type C and D panels, they were made of the compressed wood, Kevlar, Dyneema, and steel plate (thin plate for recording signature). As shown in Fig. 15 (panel C2) and Fig. 16 (panel D1), bullet hole cannot be clearly observed on the front compressed wood plate, due to the restored expansion of compressed wood. The failure mode on the back steel plate with a clear hole for both panels are similar. Fig. 17 shows that panel $E_1$ was not perforated by the projectile, just with a doom signature on the back steel plate. However, the front ceramic tile was completely smashed with radial cracks, as expected.

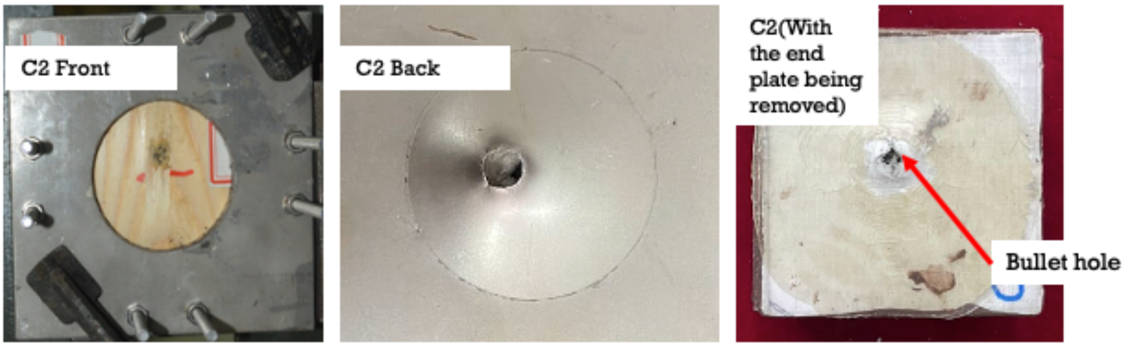


Fig. 15. Failure mode of C2 (5 mm compressed wood + 2 mm × 5 plates Kevlar + 2 mm × 5 plates Dyneema + 2 mm × 5 plates compressed wood with a 2 mm steel plate): the front face (left), back face (middle) and with back plate being removed (right).


Fig. 16. Failure mode of D1 (15 mm compressed wood + 5 mm Kevlar + 5 mm Dyneema with a 2 mm steel plate): the front face (left), back face (middle) and with back plate being removed (right).

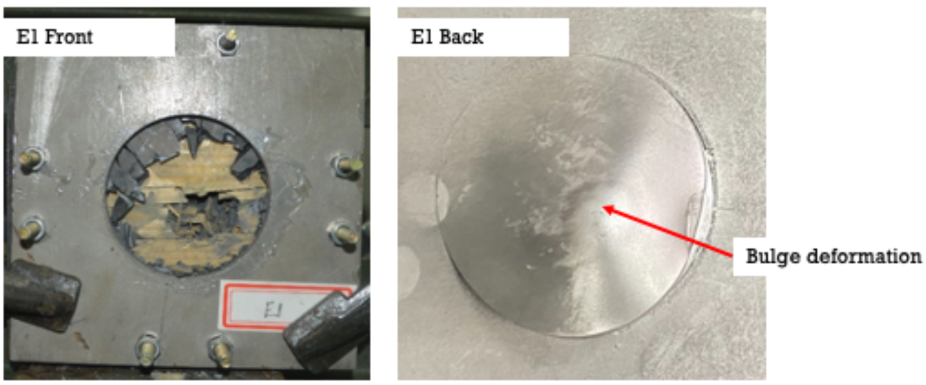


Fig. 17. Failure mode of E1 (5 mm SiC + 4.8 mm compressed wood + 5 mm $B_4C$ + 2.25 mm Dyneema with a 2 mm steel plate): the front face (left) and back face (right).

Type F panels were used to show ballistic behaviour of a single material to provide basic data for validating analytical models and calibrating computer models. Figs. 18 and 19 show the failure modes of 10 mm SiC panel (F1) without any back plate and 10 mm $B_4C$ panel with a 2 mm back steel plate (F2). The SiC ceramic panel was completely smashed (Fig. 18), as expected, due to no back steel plate. The front face of $B_4C$ ceramic layer was fragmented along the radial directions originated from the striking location and there was a bullet hole in the centre (Fig. 19). The back steel plate showed a ductile failure mode with a bulge deformation and a bullet hole.

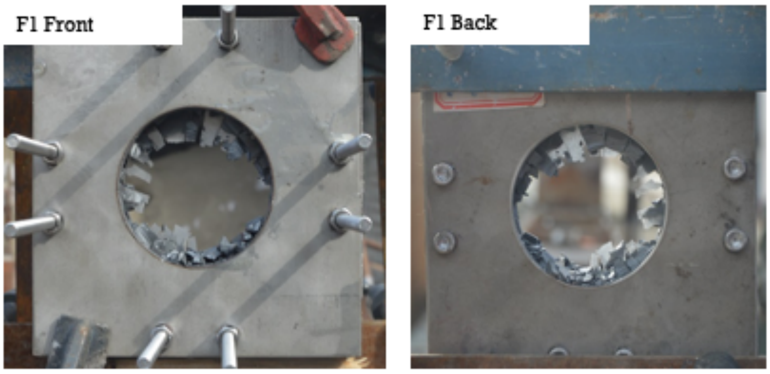


Fig. 18. Failure mode of F1 (10 mm SiC): the front face (left) and back face (right).

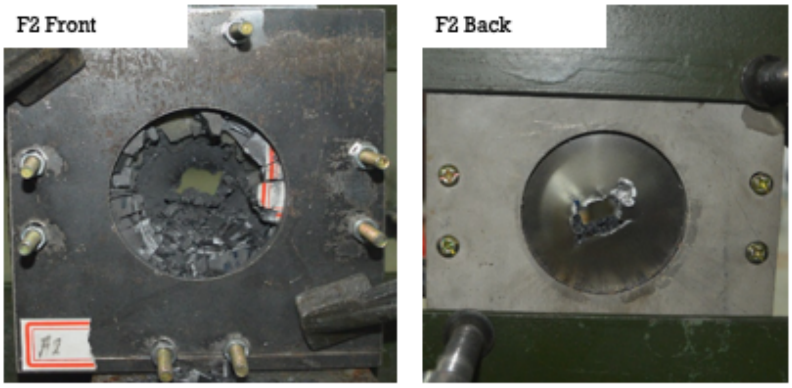


Fig. 19. Failure mode of F2 (10 mm $B_4C$): the front face (left) and back face (right).

Figs. 20 and 21 show the failure modes of panel F3 (10 mm Kevlar with a 2 mm back steel plate) and panel F4 (10 mm Dyneema with a 2 mm back steel plate), respectively. It can be observed that the perforation holes at the front and back faces of Kevlar based panel (F3) are smaller than those of Dyneema based panel (F4). This is likely attributed to the different resistances offered by Kevlar and Dyneema fibres. The former has the less ballistic resistance than the latter, so that the back face signature of the former is much smaller than that of the latter, due to the less limit on the out-of-plane deformations of Kevlar.

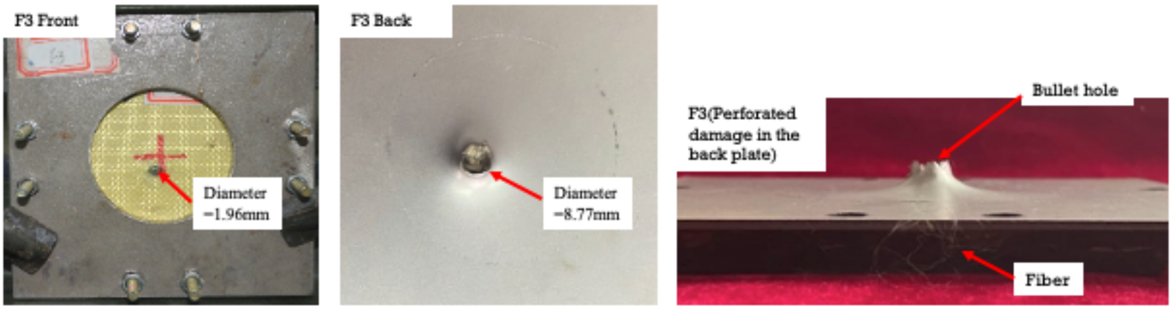


Fig. 20. Failure mode of F3 (10 mm Kevlar with a 2 mm steel plate): the front face (left), back face (middle) and perforated damage in the back plate (right).

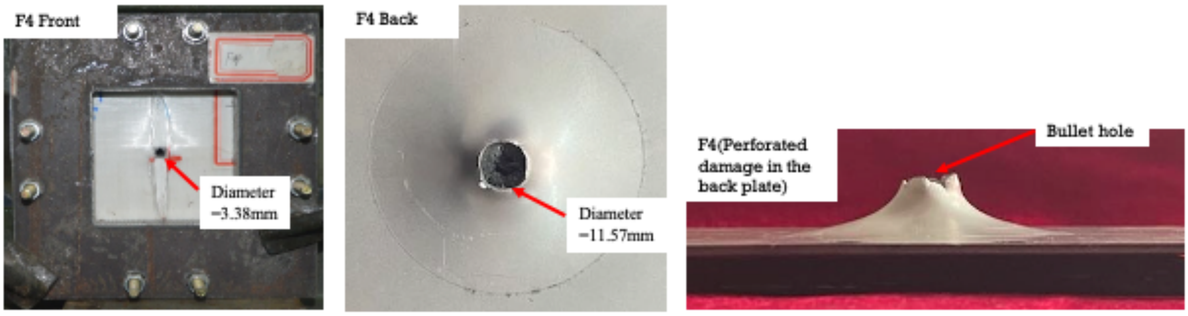


Fig. 21. Failure mode of F4 (10 mm Dyneema with a 2 mm steel plate): the front face (left), back face (middle) and perforated damage in the back plate (right).

Fig. 22 shows the failure mode of 15 mm thick CW panel, with a clear damage generated by the perforation of bullet at both the front and back faces. However, due to the high velocity impact, wood fibres closed the bullet hole on both faces. As the impact velocity was quite high which destroyed the compressed wood easily, thus the compressed wood panel had a crack through the bullet hole, as shown in Fig. 22 (CW with clamps are removed). There was hardly any permanent deformation on the compressed wood panel, as it is a brittle material. The results show that compressed wood is not an effective ballistic material without removing lignin out from the wood [31], even though its density and mechanical properties are three times of its uncompressed counterpart.

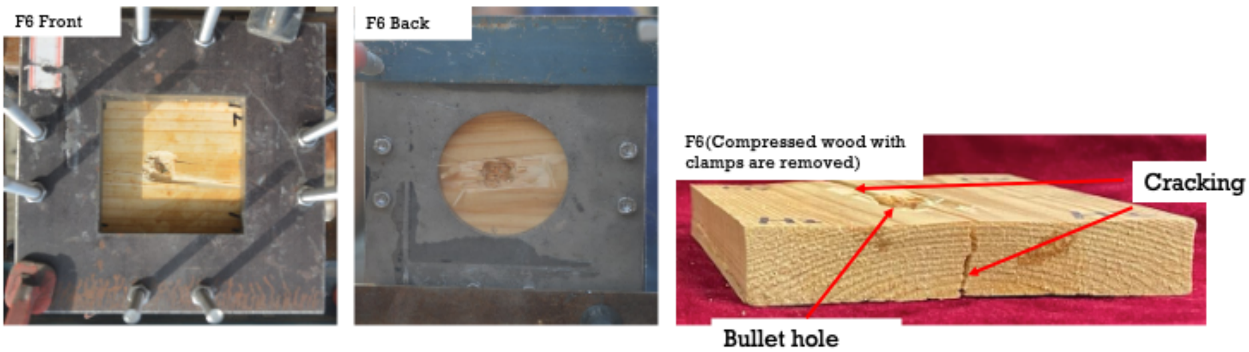

Fig. 22. Failure mode of F6 (15 mm compressed wood): the front face (left), back face (middle) and with clamps being removed (right).

### 4.3 Comparison of costs

Known the present prices of constituent materials, a guidance may be given on the effective cost of hybrid laminated panels. The unit prices of a 100 × 100 × 5 $mm^3$ SiC or $B_4C$ tile are $17.03 and $33.21 per tile, respectively, in the current market. The prices of a single piece of 100×100×45 $mm^3$ original Scots Pine wood and a 100×100×2 $mm^3$ steel plate are approximately $1.49 and $3.62 per piece, respectively. The prices of Kevlar 49 plain weave fabric and Dyneema HB210 ballistic armor UHMWPE are $54.95 and $30.99 per yard roll, respectively. The price/thickness of five hybrid panels which successfully resisted bullet is shown in Fig. 23. Thus, concerning the ballistic performance of each hybrid panels in this study, the composite panel (A5) of a 5 mm SiC tile with 10 mm Dyneema laminates is the most competitive.

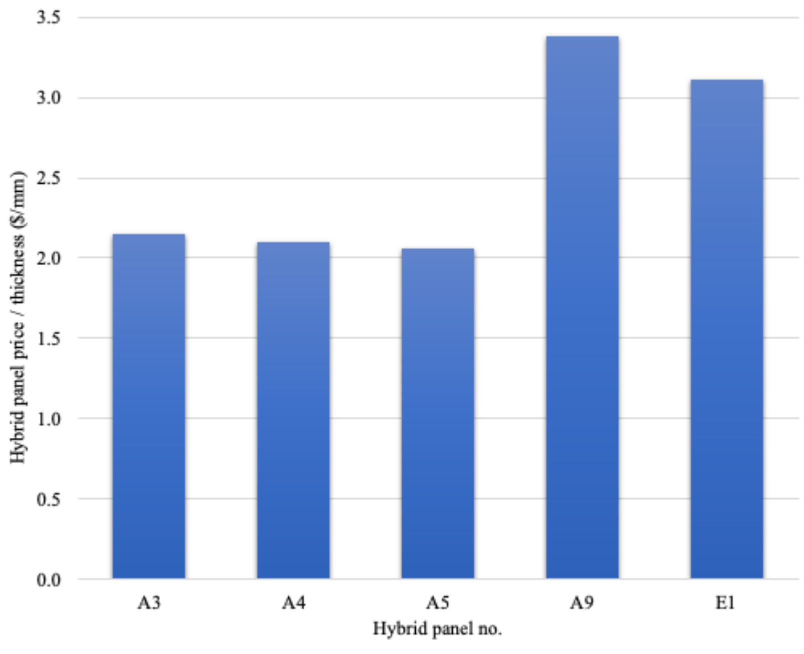


Fig. 23. Comparison of prices of various hybrid panels which successfully resisted bullet.

### 4.4 Analytical predictions

4.4.1 Determination of calculation parameters

By applying the analytical model of plain weave, ceramic, steel and compressed wood in Section 3, the key parameters of target materials can be determined according to the ballistic test results (Table

2). The parameters determined on plain weave, ceramic, steel and compressed wood are shown in Tables 4 and 5, respectively. The parameters of mechanical properties of materials used in the calculations are measured from tests, other parameters are derived from literature [27], and calibrated by comparing the simulations of composite structures subjected to ballistic impact with the experimental data under different circumstances.

Table 4. Parameters of plain weave composites used in the calculation

| Plain weave | Young's modulus (MPa) | Maximum strain of yarn | Volume density of yarn (kg/m$^3$) | Quasi-lemniscate area reduction factor | Stress wave transmission factor |
|---|---|---|---|---|---|
| Kevlar | 95 | 0.025 | 1158 | 0.8 | 0.95 |
| Dyneema | 89[32] | 0.035 | 996 | 1 | 0.95 |
| Plain weave | Delamination percent | Matrix crack percent | Mode II dynamic critical strain energy release rate(J/m$^2$) | Matrix cracking energy (MJ/m$^3$) | |
| Kevlar | 100% | 100% | 800 | 0.9 | |
| Dyneema | 100% | 100% | 900 | 1.5 | |

Table 5. Parameters of ceramic, steel and compressed wood used in calculations

| Material | Density(kg/m$^3$) | $\sigma_t$ (GPa) |
|---|---|---|
| SiC | 3200 | 4.7 |
| $B_4C$ | 2520 | 7 |
| Steel | 7830 | 0.87 |
| Compressed wood | 1200 | 0.35 |

### 4.4.2 Validation of analytical model

Table 6 shows the comparisons of the residual velocity of bullet and the bulging deformations from the back steel between the ballistic test data and the calculation results, with relatively small discrepancies. This indicates that the current analytical model is capable of providing accurate predictions. However, as the current model ignores the petal perforation of the steel back plate, the calculated bulging deformations are much smaller than those in the ballistic tests. Thus, the petal perforation may need to be considered in future.

Table 6. Comparison between ballistic test results and theoretical calculations

| Composite Panel | Back steel plate | Actual Thick-ness (mm) | Initial Velocity (m/s) | Residual velocity (m/s) | | | Bulging deformation from steel (mm) | | |
|---|---|---|---|---|---|---|---|---|---|
| | | | | Test | Cal. | Error (%) | Test | Cal. | Error (%) |
| 10mmSiC | None | 10.49 | 814.00 | 490.35 | 492.27 | 0.4 | / | / | / |
| 10mm$B_4C$ | Yes | 10.42 | 829.88 | 229.74 | 233.45 | 1.6 | / | / | / |
| 10mmK | Yes | 9.93 | 826.56 | 749.73 | 790.50 | 5.4 | 10.14 | / | / |

| | | | | | | | | | |
|---|---|---|---|---|---|---|---|---|---|
| 10mmD | Yes | 8.53 | 836.90 | 767.45 | 808.68 | 5.4 | 14.2 | / | / |
| 15mmT | None | 15.00 | 887.50 | 862.50 | 853.27 | -1.1 | / | / | / |
| 15mmT | None | 14.90 | 806.00 | 720.00 | 777.93 | 8.0 | / | / | / |
| 5mmSiC+10mmK | Yes | 15.28 | 825.00 | 201.00 | 216.59 | 7.7 | 21.82 | 20.12 | -7.8 |
| 5mmSiC+10mmD | Yes | 14.02 | 812.00 | 0 | 0 | / | 20.52 | 20.36 | -0.8 |
| 5mm$B_4C$+10mmK | Yes | 15.33 | 835.82 | 161.69 | 152.16 | -5.9 | 31.35 | 19.29 | -38.5 |
| 5mm$B_4C$+10mmD | Yes | 13.72 | 827.27 | 0 | 0 | / | 26.14 | 20.34 | -22.2 |

### 4.4.3 Prediction of energy absorption and residual velocity in composite structures

Assuming that the impact velocity of a bullet is 825 m/s, using the analytical model developed the energy absorption in fibre, total energy absorption and residual velocity against the thickness ratio of ceramic layer to fibre layer are predicted for four composite structures with an areal density of 25, 30, 35 kg/m$^2$, as shown in Figs. 24 - 26, respectively. The minimum thicknesses of a single material layer to avoid perforation are calculated as 17, 11.7, 30 and 29 mm for SiC, $B_4C$, Kevlar and Dyneema, respectively. Correspondingly, the minimum areal density of single layer to avoid perforation are 54, 29, 35 and 29 kg/m$^2$ for the above four materials, respectively.

Fig. 24(a) shows that the total energy absorbed by all composite hybrid structures increases greatly in the initial stage and reaches the highest value (kinetic energy of the bullet: 3400 J) with increasing the thickness ratio, i.e. with increasing the front ceramic thickness for the given areal density. Correspondingly, in this thickness ratio range, the residual velocity of the bullet decreases steeply to 0 m/s and then keeps there till the ratio at 0.4 for Sic/Kevlar panel and higher for other panels, as shown in Fig. 24(c). Here, the growing ballistic resistance of all composite structures is attributed to the increase of thickness of ceramic layer. The areal density of the composite structures at 25 kg/m$^2$ is lower than the minimum areal densities of a single Kevlar or Dyneema panel to avoid perforating, i.e. 34.74 kg/m$^2$ for Kevlar and 28.89 kg/m$^2$ for Dyneema. As a result, the composite structures without ceramic layer or with a very thin ceramic layer (very low thickness ratio $< 0.15$) cannot block the bullet in the low thickness ratio range. With increasing the thickness ratio to 0.4, 0.6, 0.5, 1.1 for SiC/Kevlar, SiC/Dyneema, $B_4C$/Kevlar and $B_4C$/Dyneema, respectively, the ceramic/fibre hybrid structures consume the total kinetic energy of the bullet (Fig. 24a). Consequently, the corresponding residual velocities become zero in that thickness ratio range (Fig. 24c). However, with further increasing the thickness ratio, the fibre layer becomes thinner and thinner, so that the hybrid structures lose necessary support from the fibre layer to back up the brittle ceramic layer. As a result, the total energy absorption and residual velocity of the bullet are approaching to a certain value for the hybrid composite structures with SiC and $B_4C$. It is understandable that with increasing the thickness ratio after the initial up-trend stage, the energy absorption in fibre decreases continuously, due to the fibre layer getting thinner and thinner (Fig. 24b).

When the areal density of the structures increases to 30 kg/m$^2$, it is larger than the minimum areal density of a single $B_4C$ or Dyneema layers to avoid perforation. Therefore, the $B_4C$/Dyneema structure can block the bullet at any thickness ratio since the total energy absorption remains 3400 J and residual velocity of bullet remains 0 m/s, as shown in Figs. 25(a) and 4(c). The SiC/Kevlar composite shows the similar ballistic performance when the thickness ratio is slightly above zero (0.04). Differently, the SiC/Dyneema and SiC/Kevlar can resist the impact of the bullet when the thickness ratio is up to 0.7 and 0.55, respectively. Fig. 25(b) indicates that the energy absorption in fibre on SiC/Dyneema and $B_4C$/Dyneema panels decreases with the increase of the thickness ratio from the beginning, whilst that of SiC/Kevlar and $B_4C$/Kevlar increases with the small increase of the thickness ratio, followed by a continuous decrease.

When the areal density of the hybrid structures is 35 kg/m$^2$, it is again larger than the minimum areal density of a single $B_4C$, Kevlar or Dyneema layer to avoid perforation. Therefore, the $B_4C$/Kevlar and $B_4C$/Dyneema panel can block the bullet at any thickness ratio, as shown in Figs. 26(a) and 5(c). Besides, the energy absorption in $B_4C$/Kevlar and $B_4C$/Dyneema decreases to 0 J, since the bullet is blocked by the ceramic layer at the front face when the thickness ratio is larger 2.5, as shown in Fig. 26b. For SiC/Kevlar and SiC/Dyneema panels, the total energy absorption decreases and the residual velocity increases approaching to a constant value, with the further increase of the thickness ratio from 0.7 and 0.9, respectively.

The calculation results show that at a relatively low areal density (e.g. 25 kg/m$^2$), the thickness ratio has an optimal range to avoid being perforated. With the increase of areal density of the composite structures, the thickness ratio offers limited effects on the ballistic performance of the composite structures. This indicates that the energy absorption in the composite structures investigated has a coupling effect in energy absorption between fibre and ceramic layers. The results manifest that an optimal thickness ratio of ceramic to fibre layers exists in the composite structures studied. The increase of fibre layer can enhance the ballistic performance of the composite structure at a relatively low areal density. However, as the fibre layer consumes the kinetic energy of bullet through the large deformations, the thick fibre layer may cause damage in the object placed behind due to a large back face signature.

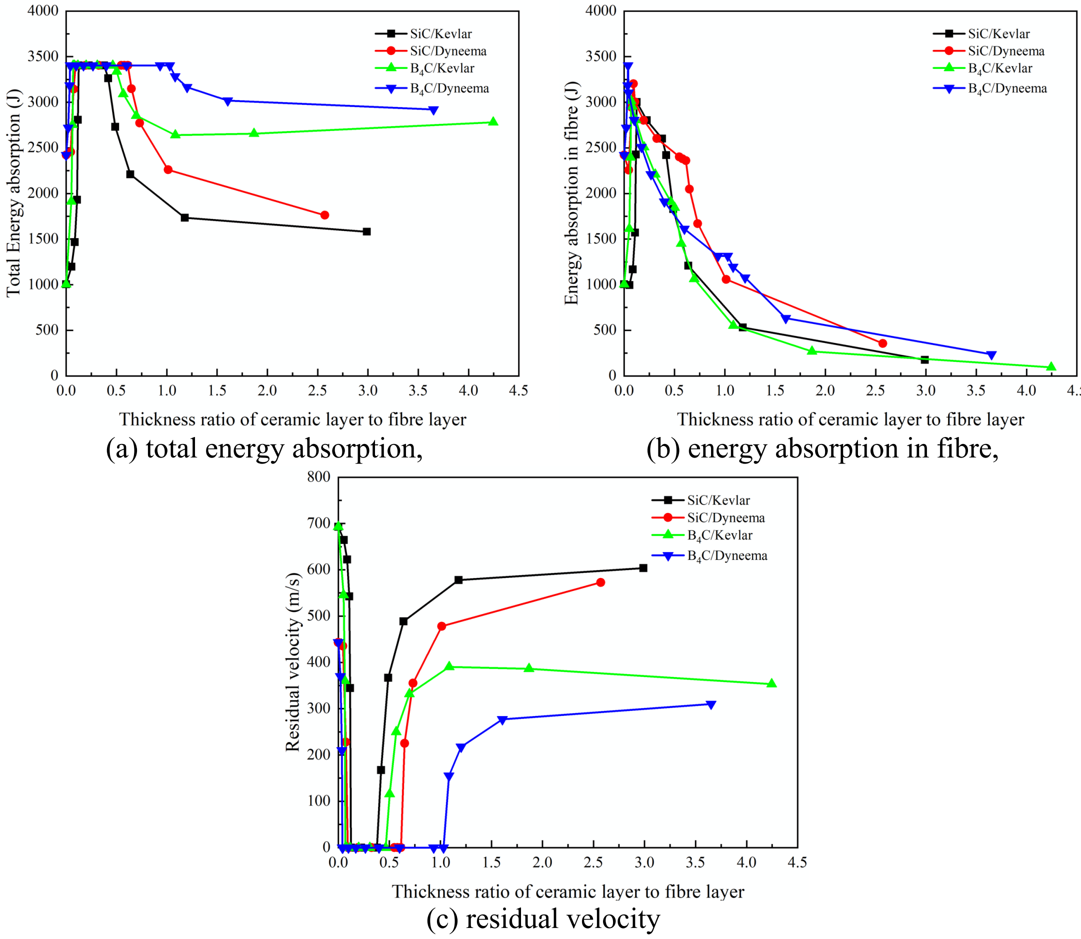


Fig. 24. Predictions of ballistic performance of four composite hybrid structures with an areal density of $25 kg/m^2$.

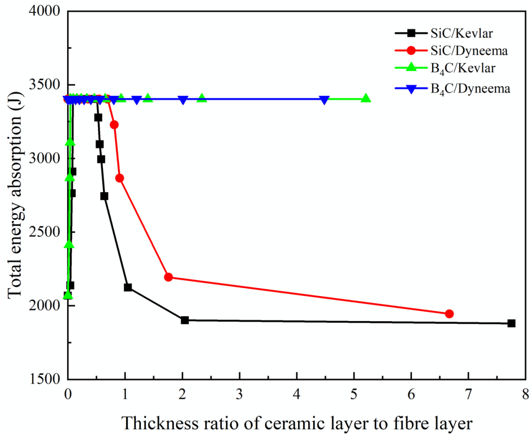


(a) total energy absorption,

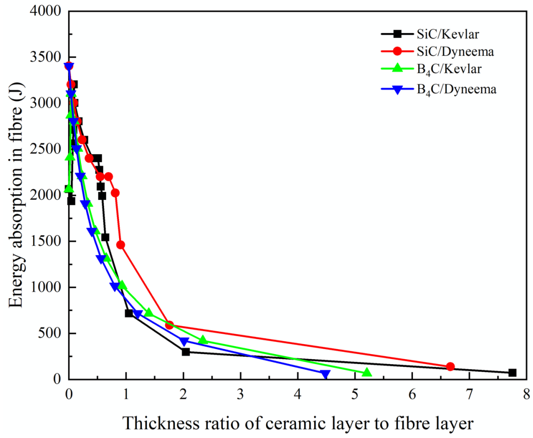


(b) energy absorption in fibre,

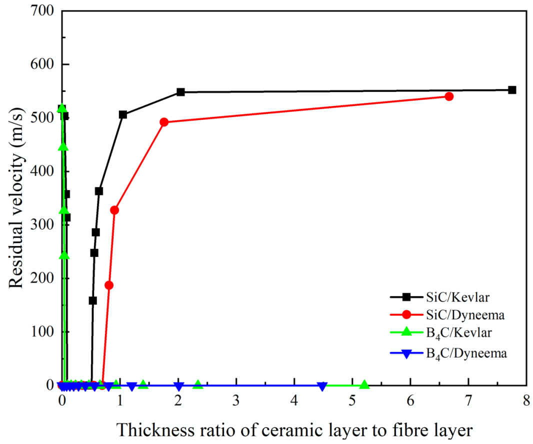


(c) residual velocity

Fig. 25. Predictions of ballistic performance of four composite hybrid structures with an areal density of 30 kg/m$^2$.

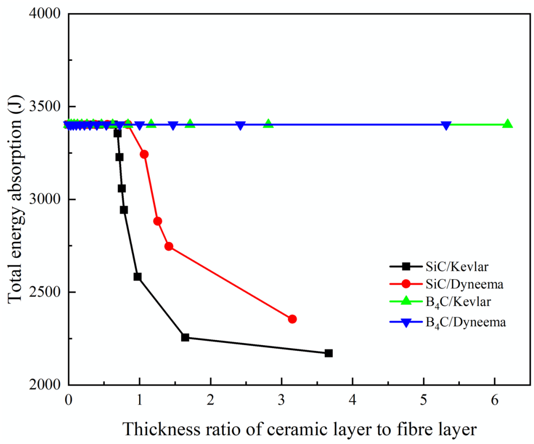


(a) total energy absorption,

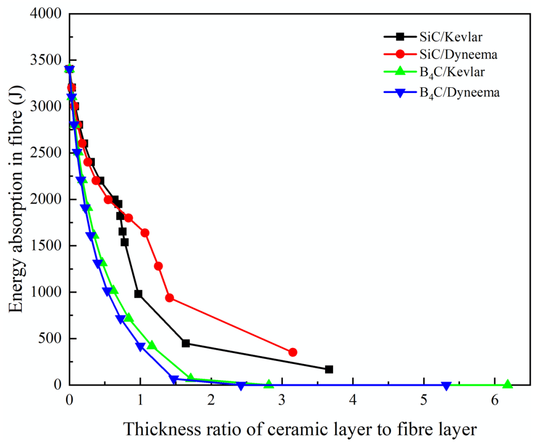


(b) energy absorption in fibre,

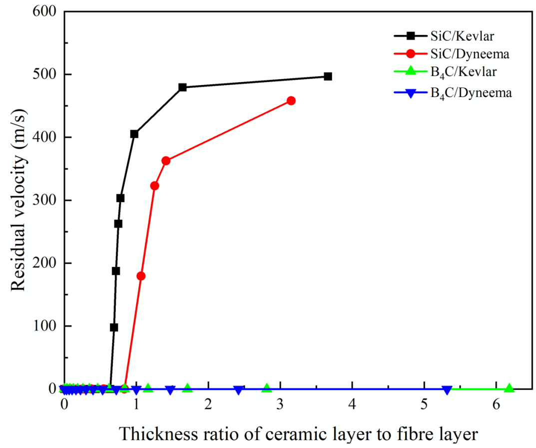

(c) residual velocity

Fig. 26. Predictions of ballistic performance of four composite hybrid structures with an areal density of 35 kg/m$^2$.

## 5 Conclusions

Through the current experimental work, various hybrid ballistic laminated panels have been developed and tested, with their ballistic behaviour being assessed and promising panels being identified. The details of panel design and manufacturing have been given. Together with the corresponding ballistic performance, the research outputs provide the first-hand data on ballistic impact resistance of hybrid laminated and single material panels. There have been fourteen types, in total 19 hybrid and 6 single material panels, being tested against high velocity impact by a 7.62 mm projectile. Five hybrid panels have successfully resisted the bullet, whilst twenty panels have been perforated with various residual velocities. Based on the ballistic results, $B_4C$-Dyneema composite panel (A9) has delivered the best ballistic performance with the lowest areal density and thickness, compared with other four partial penetration panels.

As for the material failure modes, the front ceramic tiles were fragmented into small pieces along the radial cracks originated from the striking centre. Moreover, both Kevlar and Dyneema backing materials offer a good ballistic resistance after the bullet is blunted by the front hard ceramic tile, which is reflected by drawn-in of the material at the clamping boundary of the panels. There is clearly a bullet hole at Dyneema laminates, but such the hole is closed on Kevlar laminates, due to the different ballistic resistances offered by these two materials. In addition, if the thickness of fabric panels is the same, the bulged deformation of the Dyneema is normally greater than that of Kevlar due to the higher limit on the out of plane deformation. As for the compressed wood, although it is one of lightweight materials, its ballistic performance and energy absorption are poor.

Analytical models are also developed to predict ballistic perforation performance of single material layers and the related hybrid composite structures. The theoretical predictions of residual velocities are validated against the corresponding experimental measurements, with reasonably good correlation. However, the predictions of bulging deformations for boron carbide-based hybrid panels are of relatively large discrepancies, due to ignoring the petal formations of the back steel plate. The parametric studies are also undertaken to predict the total energy absorption, energy absorption in fibre and residual velocity related to four hybrid composite structures with three areal densities, providing interesting discussion.

The research outputs produced in the ballistic impact tests provide the key experimental data, in terms of bulge deformation, residual velocity and failure mode, together with the theoretical models, which can be used to help design such the hybrid ballistic panels.

## Data availability

The raw/processed data required to reproduce these findings cannot be shared at this time as the data also forms part of an ongoing study.

## Acknowledgements

The authors gratefully acknowledge the financial support from the China Scholarship Council (CSC) and Youth Science and Technology Growth Projects of Guizhou Province Education Department (NO. QJH KY2018301). This research is supported by the Program of Introducing Talents of Discipline to University (NO. B16025).

Also, the authors would like to thank Dupont Company and DSM Company for supplying Kevlar® and Dyneema® samples.

## References

[1] Jones RM. *Mechanics of composite materials.,* London: Taylor & Francis, 1999.

[2] Krishnan K, Sockalingam S, Bansal S, Rajan SD. Numerical simulation of ceramic composite armor subjected to ballistic impact. Composites Part B: Engineering 2010; 41(8): 583-93.

[3] Liu W, Chen Z, Cheng X, Wang Y, Amankwa, AR, Xu J. Design and ballistic penetration of the ceramic composite armor, Composite Part B: Engineering 2016; 84: 33-40.

[4] Hu D, Zhang Y, Shen Z, Cai Q. Investigation on the ballistic behaviour of mosaic SiC/UHMWPE composite armor systems, Ceram Int 2017; 43(13): 10368-76.

[5] Serjouei A, Gour G, Zhang X, Idapalapati S, Tan GEB. On improving ballistic limit of bi-layer ceramic-metal armor, Int J Impact Eng 2017; 105: 54-67.

[6] Horsfall I, Austin SJ, Bishop W. Structural ballistic armour for transport aircraft. Int J Materials & Design 1999; 21(1): 19-25.

[7] Islam MRI, Zheng JQ, Batra RC. Ballistic performance of ceramic and ceramic-metal composite plates with JH1, JH2 and JHB material models. Int J Impact Eng 2020; 137: Article 103469.

[8] Backman ME, Goldsmith W. The mechanics of penetration of projectiles into targets. Int J Eng Sci 1978; 16(1): 1-99.

[9] Wilkins ML. Mechanics of penetration and perforation. Int J Eng Sci 1978; 16(11): 793-807.

[10] Crouch IG. Body armour - New materials, new systems, Defence Technol 2019; 15(3): 241-53.

[11] Liu W, Chen Z, Chen Z, Cheng X, Wang Y, Chen X, Liu J, Li B, Wang S. Influence of different back laminate layers on ballistic performance of ceramic composite armor, Materials & Design 2015; 87: 421-427.

[12] Shen Z, Hu D, Yang G, Han X. Ballistic reliability study on SiC/UHMWPE composite armour against armour-piercing bullet, Composite Struct 2019; 213: 209-19.

[13] Zhang Y, Dong H, Liang K, Huang Y. Impact simulation and ballistic analysis of $B_4C$ composite armour based on target plate tests, Ceram Int 2021; 47(7): 10035-49.

[14] Dinwoodie JM. *Timber: its nature and behaviour.,* 2ed ed. London: E & FN Spon, 2000.

[15] Alinoori F, Sharafi P, Moshiri F, Samali B. Experimental investigation on load bearing capacity of full scaled light timber framed wall for mid-rise building, Construction and Building Materials 2020; 231: Article 117069.

[16] Ling Z, Liu W Shao J. Experimental and theroretical investigation on shear behaviour of small-scale timber beams strengthened with Fibre-Reinforced Polymer composites, Composite Structures 2020; 240: Article 111989.

[17] Sotayo A, Bradley D, Bather M, Sareh P, Oudjene M, El-Houjeyri I, Harte AM, Mehra S, O˙Ceallaigh C, Haller P, Namari S, Makradi A, Belouettar S, Bouhala L, Deneufbourg F, Guan ZW. Review of state of the art of dowel laminated timber members and densified wood materials as sustainable engineered wood products for construction and building applications, Construction and Building Materials 2020; 1: Article 100004.

[18] Bodig J, Jayne B. *Mechanics of wood and wood composites.,* New York: Van Nostrand Reynold company, 1982.

[19] Da Silva A, Kyriakides S. Compressive response and failure of balsa wood, Int J Solid Struct 2007; 44(25-26): 8685-717.

[20] Wei J, Rao F, Zhang Y, Yu W, Hse C, Shupe T. Laminating wood fibre mats into a densified material with high performance, Materials Letters 2019; 253: 358-61.

[21] Bekhta P, Salca E, Lunguleasa A. Some properties of plywood panels manufactured from combinations of thermally densified and non-densified veneers of different thickness in one structure, J Building Eng 2020; 29: Article 101116.

[22] Kutnar A, Sandberg D, Haller P. Compressed and moulded wood from processing to products, Holzforschung 2015; 69(7): 885-97.

[23] Sanborn K, Gentry TR, Koch Z, Valkenbury A, Conley C, Stewart LK. Ballistic performance of Cross-laminated Timber (CLT), Int J Impact Eng 2019; 128: 11-23.

[24] Maffeo M, Cunniff PM. Composite materials for small arms (ball round) protective armour, Revolut Mater Technol Econ 2000; 32: 768-77.

[25] Ong CW, Boey CW, Hixson RS, Sinibaldi JO. Advanced layered personnel armor, Int J Impact Eng 2011; 38(5): 369-83.

[26] Braga FO, Bolzan LT, Luz FS, Lopes PHLM, Jr EPL, Monteiro, SN. High energy ballistic and fracture comparison between multilayered armor systems using non-woven curaua fabric composites and aramid laminates, J Materials Research Technol 2017; 6(4): 417-22.

[27] Naik NK, Shiriraom P. Composite structures under ballistic impact. Composite Structures, 2004, 66(1/4):579-590.

[28] Gu B. Analytical modeling for the ballistic perforation of planar plain-woven fabric target by projectile. Composite: Part B. 2003, 34: 361-371.

[29] Nguyen LH, Lassig TR, Ryan S, Riedel W, Mouritz AP, Orifici AC. A methodology for hydrocode analysis of ultra-high molecular weight polyethylene composite under ballistic impact, Composites Part A: Applied Sci & Manufacturing 2016; 84: 224-35.

[30] Ballistic Resistance of Body Armor NIJ Standard-0101.06. National Institute of Justice Office of Science and Technology Washington, DC 20531, 2008.

[31] Song J, Chen C, Zhu S, Zhu M, Dai J, Ray U, Li Y, Li Y, Quispe N, Yao Y, Gong A, Leister UH, Bruch H, Zhu JY, Vellore A, Li H, Minus ML, Jia Z, Martini A, Li T, Hui L. Processing bulk natural wood into a high – performance structural material, Nature 2018; 554: 224-28.

[32] O'Masta MR, Deshpande VS, Wadley HNG. Mechanisms of projectile penetration in Dyneema encapsulated aluminum structures. International Journal of Impact Engineering. 2014, 74:16-35.